Effect of Ce³⁺ on the morphology, composition, and thermal properties of single and core-shell polyethylene oxide electrospun fibers

L. A. Hoyos-Lima, V. Altuzar, J. F. Perzábal-Domínguez, S. Muñoz-Aguirre,

A. Y. Tenorio-Barajas, M. A. Palomino-Ovando, and C. Mendoza-Barrera*

Facultad de Ciencias Físico Matemáticas, Benemérita Universidad Autónoma de Puebla,

Puebla 72570, Mexico.

e-mail: cmendoza@fcfm.buap.mx

Cerium polymeric composites have novel applications in fuel cells, optical devices, gas sensors, catalysis, ultraviolet absorbers, hydrogen storage materials, and biomedicines. This study reports the fabrication of low-cost electrospun single and core-shell polyethylene oxide (PEO) doped with cerium fibers fabricated in two moisture ambients related to the fiber morphology. Scanning electron microscopy and atomic force microscopy revealed that obtaining the thinnest average fiber diameter requires 47-52% RH and 2% cerium dopant. Using a PEO capping (shell fiber) allows the increment of cerium in the inner matrix (core-fiber) to produce non-beading continuous fibers with 3.5% of the dopant. The undoped single or core-shell fibers presented a 52.7 to 54.2% crystallinity, independently of relative humidity used during the fabrication process. In contrast, the use of cerium dopant up to 2% induces an increase in their crystallinity due to the formation of Ce-O species, enhancing their thermal properties, regardless of the moisture during manufacturing, as was found with Fourier transform infrared spectroscopy, differential scanning calorimetry, and thermogravimetric analysis.

1. Introduction

The electrospinning technique can fabricate several types of organic, inorganic, or composite fibers and nanofibers. By controlling the physicochemical parameters of both the spinnable solution and the ambient parameters during the fabrication process, it is possible to generate smooth, porous, hollow, filled, ribbonlike, branched, single, core-shell fibers and nanofibers, among other morphologies and architectures. Both fiber diameter and morphology allow adjusting their properties [1]. Electrospinning has been proven capable of processing several polymers and composite solutions into continuous fibers to fabricate large membranes. A fundamental requirement is to focus on polymer selection and its physicochemical properties such as molecular weight, viscosity, conductivity, and thermal [2]. Besides that, other factors that can influence fiber morphology and their properties are the electrospinning parameters such as distance to the collector, voltage, feed rate, etc. [3], and the ambient conditions (humidity, temperature, pressure, etc.) [2]. Specifically, relative humidity (RH%) could affect the morphology, structure, and diameter size distribution of the fibers [4, 5]. Several biopolymers or synthetic polymers could be selected as co-spinning agents during composite fiber fabrication as a matrix or to reinforce the material where the phase or element of interest may intercalate [6]. One of these polymers is the poly(ethylene oxide), PEO, used to facilitate polymer entanglement during electrospinning production due to its linear structure with flexible and long chains [7]. Cerium, in turn, is the most abundant lanthanide found on Earth, which

shows stability at both trivalent and tetravalent states. It has been used in fuel cells, optical devices, gas sensors, catalysis, ultraviolet absorbers, hydrogen storage materials, polishing materials, and biomedical applications [8]. William *et al.* reported that Ce ions increase the electrical charge and evaporation rate during the Electrospinning process in PEO solutions [9]. Meanwhile, mix-ups of cerium (III) nitrate hexahydrate and poly ethylene glycol inhibit the corrosion of a cathode during an immersion period of at least 30 min [10]. Likewise, the interaction of Ce dopant exhibits a prolonged antimicrobial activity due to its dual oxidation state. It has low levels of toxicity in fibroblasts, so its cutaneous use is plausible [11]. This work establishes the experimental conditions to fabricate single and core-shell fibers of PEO doped with cerium chloride hexahydrate III (Ce) at several concentrations in two ambient humidities.

Their morphology, average diameter, composition, and thermal properties were analyzed using scanning electron microscopy (SEM), atomic force microscopy (AFM), Fourier transform infrared spectroscopy (FTIR), differential scanning calorimetry (DSC), and thermogravimetric analysis (TGA).

2. Materials and Methods

2.1. Materials

Polyethylene oxide (PEO, $(\text{-CH}_2\text{CH}_2\text{O-})_n$, $M_W = 600,000$ g/mol), cerium (III) nitrate hexahydrate (Ce, $\text{Ce(NO}_3)_3\cdot6\text{H}_2\text{O}$, $M_W = 434.22$), and acetic acid (Ac.Ac., CH_3COOH) were purchased from Sigma-Aldrich. We used

TABLE I. Sample nomenclature of fibers manufactured by electrospinning technique. The out layer of all core-shell samples is PEO at 4 %. Letter s or d refers to single and core-shell fiber, H or L to 47-52 and 27-32 %RH, and 0, 0.5, 2, or 35 refer to the concentration of the Ce molar ratio used (0, 0.5, 2.0, and 3.5 %).

Type of fiber	RH (47-52 %)	RH (27-32 %)	Molar ratio
Single	PEOCeHs0	PEOCeLs0	PEO/Ce (0%)
Single	PEOCeHs05	PEOCeLs05	PEO/Ce (0.5%)
Single	PEOCeHs2	PEOCeLs2	PEO/Ce (2%)
Single	PEOCeHs35	PEOCeLs35	PEO/Ce (3.5%)
Core-shell	PEOCeHd0	PEOCeLd0	PEO/Ce (0%)
Core-shell	PEOCeHd05	PEOCeLd05	PEO/Ce (0.5%)
Core-shell	PEOCeHd2	PEOCeLd2	PEO/Ce (2%)
Core-shell	PEOCeHd35	PEOCeLd35	PEO/Ce (3.5%)

deionized water grade miliQ (ddH$_2$O) with electrical resistivity of 18.2 MΩ·cm. All reagents were analytical grade and used without any purification.

2.2. Preparation of single and core-shell fibers

Acetic acid at 10 %v/v was used to dissolve 4 % of PEO under vigorous stirring for 2 h at room temperature to prepare the core solution of the bilayer and single fibers. After a minimum of 12 h, Ce at 0, 0.5, 2.0, or 3.5 % was added to the previous solution and vigorously stirred at room temperature for 1 h. The outer layer of the core-shell samples was made only of 4 % PEO solutions. A homemade electrospinning system manufactured the samples in two relative humidity ranges (RH = 27-32% and 47-52%) monitored with Labview® Software [2, 5, 8]. Single (21G×30 mm) or core-shell (21G×30 and 18G×40 mm) spinnerets were used to fabricate them (Fig. 1). The aqueous polymer solutions of interest were injected with a programmable pump (KD Scientific^{TM}, model: 780100V) loaded into a single or double syringes system. The needle tip was connected to the anode of the voltage power supply (Gamma High Voltage Research,
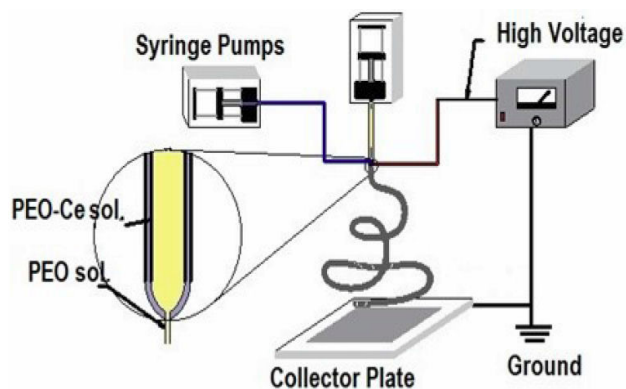

FIGURE 1. Schematic experimental setup of the homemade coaxial electrospinning.

model: ES60p-20W/DAM), whereas the cathode was attached to an aluminum collector of 10×10 cm. The values of the variables: electrode separation ($d = 14$ cm), voltage ($V = 20 - 25$ kV DC), core infusion rate ($v_i = 0.03$ mL/h), and shell infusion rate ($v_e = 0.06$ mL/h) in the bilayer samples, and $v = 0.02 - 0.8$ mL/h in the single fibers were experimentally determined after optimizing the processing parameters. All the experiments were carried out at normal pressure and temperature, replicated three times, and stored in a desiccator for further analysis.

Table I summarizes the sample names, relative humidity, and the molar ratio used during the fabrication of all-fiber samples by electrospinning. PEO/Ce indicates the relation between polymer and dopant. The samples were named PEOCeXYZ, where X is s (single) or d (core-shell) sample type, Y corresponds to the percentage of relative humidity used inside the chamber during the fabrication ($H = 47 - 52$ and $L = 27 - 32$ %RH), whereas Z is the concentration of Ce used (0, 0.5, 2.0, or 3.5 %).

2.3. Characterization

The morphological characteristics of the samples were visualized with scanning electron microscopy (SEM, JSM-6610LV) in SEI mode and atomic force microscopy (AFM, XE7 de Park Systems) in tapping mode with slow scanning speed. The average fiber diameter was calculated using ImageJ® software by measuring 100 fibers in 10 SEM micrographs (X5,000) of each sample analyzed. Fourier Transform infrared spectroscopy spectra were recorded on a Thermo Scientific spectrometer (model Nicolet Isso FT-IR) with ATR apparatus, in the 4000-500 cm^{-1} range, with a 4 cm^{-1} and 32 scans per minute. Thermal properties were recorded by differential scanning calorimetry (DSC, Q2000 TA Instruments), with a heating rate of $10°$/min from 25 to $550°$C.

3. Results and discussions

To examine the spinnability of PEO/Ce solution and the influence of the addition of Ce (0, 0.5, 2, and 3.5 %) during the fabrication of single and core-shell fibers, a group of variables to fabricate polymeric scaffolds were experimentally established. Relative humidities (27-32 and 47-52 %RH), electrode separation ($d = 14$ cm), voltage ($V = 20 - 25$ kV DC), core infusion rate ($v_i = 0.03$ mL/h), and shell infusion rate ($v_e = 0.06$ mL/h) in the core-shell samples, and $v = 0.02 - 0.8$ mL/h in the single fibers allows the fabrication of fibers with no dripping during the process. Were used solutions of PEO at 4 % to fabricate the outer shell fiber in all the core-shell samples (Table I).

3.1. Morphological analysis

Single (PEO/Ce) system. In the case of single fiber scaffolds, the samples PEOCeLs0 (Ce 0 %, 27-32 %RH), PEOCeLs05
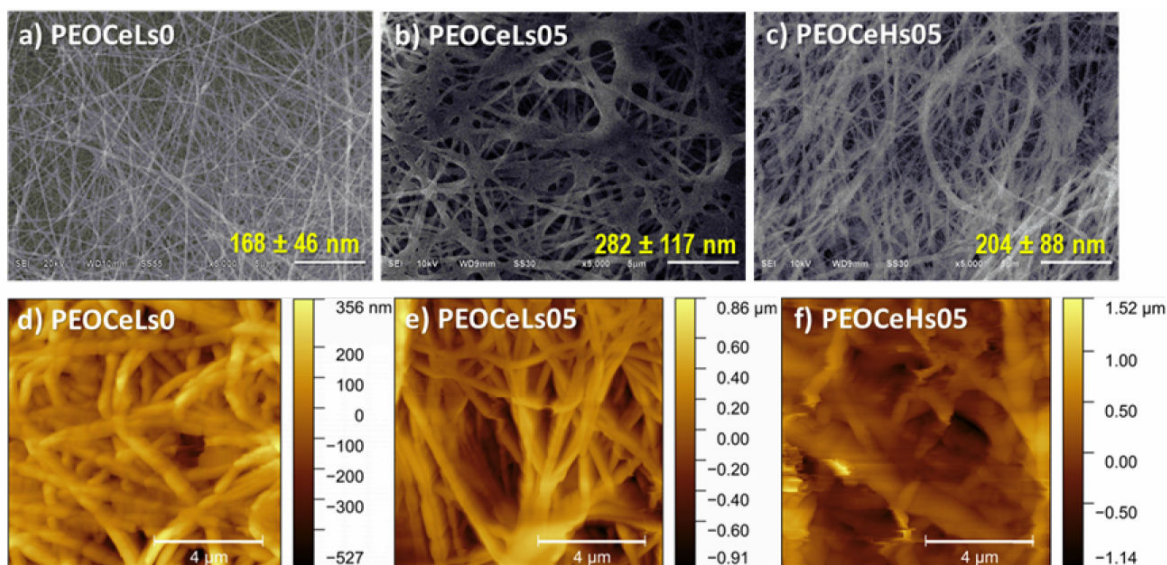
FIGURE 2. SEM (upper row) and AFM (bottom row) images of single samples: a) and d) PEOCeLs0, b) and e) PEOCeLs05, and c) and f) PEOCeHs05.

(Ce 0.5 %, and 27-32 %RH), and PEOCeHs05 (Ce 0.5 %, 47-52 %RH) showed the formation of the Taylor cone and no dripping of the needle (Fig. 2).

Undoped PEO fibers ((PEOCeLs0 sample) presented their characteristic random cylindrical shape (Fig. 2a)) [12–14]. In turn, fibers doped with Ce at 0.5 % allow the fabrication of single fibers, as previously reported [15]. PEO-CeLs0 and PEOCeLs05 single fiber composites with the lowest range of Ce exhibited a change of morphology from cylindrical fibers (Fig. 2c)) to 2D-mesh (Fig. 2b)). Depending on the application, 1D or 2D fibers are desired. AFM topography images revealed a detailed morphology of segmented cylindrical shape for PEOCeLs0 (Fig. 2d)), segmented bifibrillar in PEOCeLs05 (Fig. 2e)), and cylindrical fibers with two diameters in PEOCeHs05 (Fig. 2f)). Despite the relative humidity used during the fabrication process (27-32 or 47-52 %RH), PEO/Ce solutions with a higher dopant amount up to 0.5 % were not spinnable.

Core-shell (PEO-PEO/Ce) system. To generate a lower liquid-liquid interfacial tension between the inside and the outside to create thinner fibers, we used the same miscible acetic acid solution as a solvent [16, 17] of the PEO polymer. Several authors have prepared fibers from two immiscible polymers but miscible solvents, obtaining highly porous structures [18]. Figure 3 shows the PEO-PEO/Ce samples fabricated by coaxial electrospinning.

In all cases, primarily cylindrical fibers or 2D-mesh were found and, in some cases, some beads (Fig. 3j)). Depending on the application of fibers, a specific morphology is desirable. AFM topography images showed that the increase of Ce dopant softens and homogenizes the diameter of the threads in environments with 30 %RH. It was found that a shell capping of PEO on PEO-Ce fibers helps to increase the Ce concentration from 0.5 to 2 % under a $47 - 52$ %RH, whereas

if moisture decreases to $27 - 32$ %RH, the Ce concentration ranges from 0.5 to 3.5 %. In particular, when a 3.5 % of Ce was used (at $47-52$ %RH), the jet showed dripping, and high instability, and the Taylor cone did not form. Sharma *et al*. found 3.5% of Ce amount as the optimum amount in the case of PVA-chitosan composites [19]. The Ce amount equal to 2% produces continuous and bead-free samples for the two moisturizers used in this work.

Figure 4 shows the AFM phase and SEM micrographs (X20,000) of fibers with the highest (PEOCeLd35, 3.5 %, Fig. 4a)-b) and the lowest (PEOCeLd0, 0 %, Fig. 4c)-d) amount of dopant fabricated at 27-32 %RH. AFM phase imaging is a powerful tool to determine the presence of two materials during composite material formation, mainly in plane surfaces [20]. Here, it was applied to show the fibers bilayer when was used the same solvent on core and shell solutions for the fabrication process (Fig. 4c), black arrow) [21]. AFM phase images of Figs. 4a) and c) correspond to the AFM morphology ones of Figs. 3e) and h).

Average diameter of single and core-shell fibers. Figure 5 compares the average diameter ($p < 0.05$) of both types of fabricated samples: single and core-shell ones manufactured at two ranges of humidities ($27 - 32$ and $47 - 52$ %RH).

PEOCeLs0 and PEOCeLs05 single fiber composites (Fig. 5a)) increased on their average diameter when the relative humidity was decreased to 27-32 %RH, independently of the presence of Ce. A slightly lower average diameter was shown when moisture increases from 27-32 to 47-52 %RH (samples PEOCeLs05 and PEOCeHs05), which agrees with other authors [5,8]. Due to the PEO hydrophilicity character, increasing water molecules during the fabrication process increases the polymer jet's wettability, leading to small diameter fibers [22]. The determination of the average diameter of single samples is provided as supplementary information
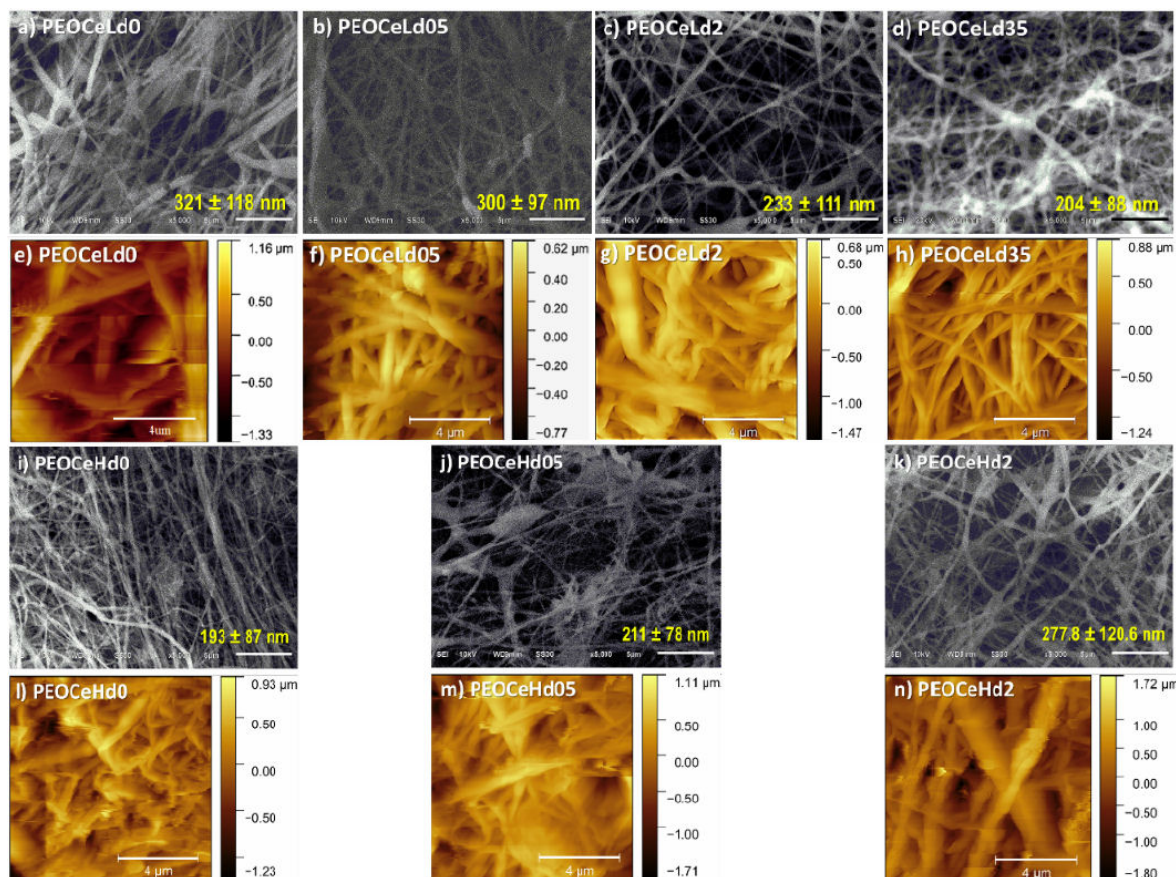
FIGURE 3. SEM (upper and third rows) and AFM (second and bottom rows) images of core-shell samples at 27-32 and 47-52 relative humidities: a) and e) PEOCeLd0, b) and f) PEOCeLd05, c) and g) PEOCeLd2, d) and h) PEOCeLd35, i) and l) PEOCeHd0, j) and m) PEOCeHd05, k) and n) PEOCeHd2.
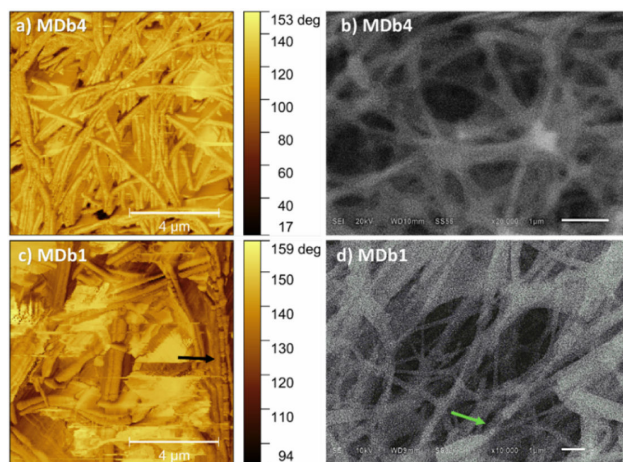

FIGURE 4. AFM phase (left column) and SEM (right column) images of core-shell samples: a-b) PEOCeLd35, and c)-d) PEO-CeLd0.

(Fig. 9). Figure 5 corresponds to the core-shell fibers fabricated at two humidity amounts in the atmosphere during the process of electrospinning (27-32 and 47-52 %RH). In this case, the linear chain of PEO or its hydrophilic character does not favor the formation of smaller diameter fibers when the water amount in the atmosphere increases (PEOCeLd0 and PEOCeHd0 samples). However, the Ce dopant in the fabrication solution, independent of the ambient water content, leads to thinner fibers. At higher humidity in the ambient (47-52 %RH), adding the lower amount of Ce results in the thinnest fibers (Fig. 5b), red boxes). It was reported that the presence of metal ions reduces both the diameter of the threads and the number of imperfections [23]. At the same time, the higher percentage of water molecules in the complexes would allow the formation of hydrogen bonds between the polymer chains [24]. The average diameter of core-shell samples is supplementary information (Fig. 10). Then, as other authors have also obtained [2, 6, 11], we observed the dependency of ambient relative humidity during the fabrication process versus fiber formation. A schematic proposal of single and core-shell fibers and the ionic interaction between the chain of PEO and cerium (III) nitrate hexahydrate is proposed in Fig. 11.

3.2. Compositional Analysis

Single PEO/Ce system. The FTIR spectra were used to determine the molecular interactions for PEO/Ce single fibers. Figure 6 shows the spectra of fiber precursors (Fig. 6a)) and
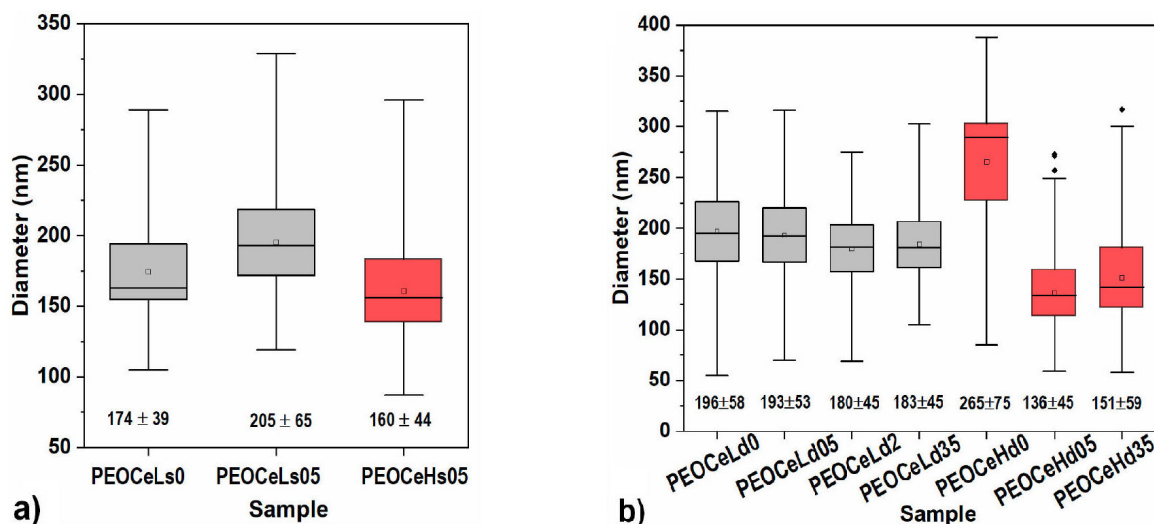
FIGURE 5. Average diameters of a) single and b) core-shell fibers fabricated at two ranges of humidities (27-32 and 47-52 %RH).
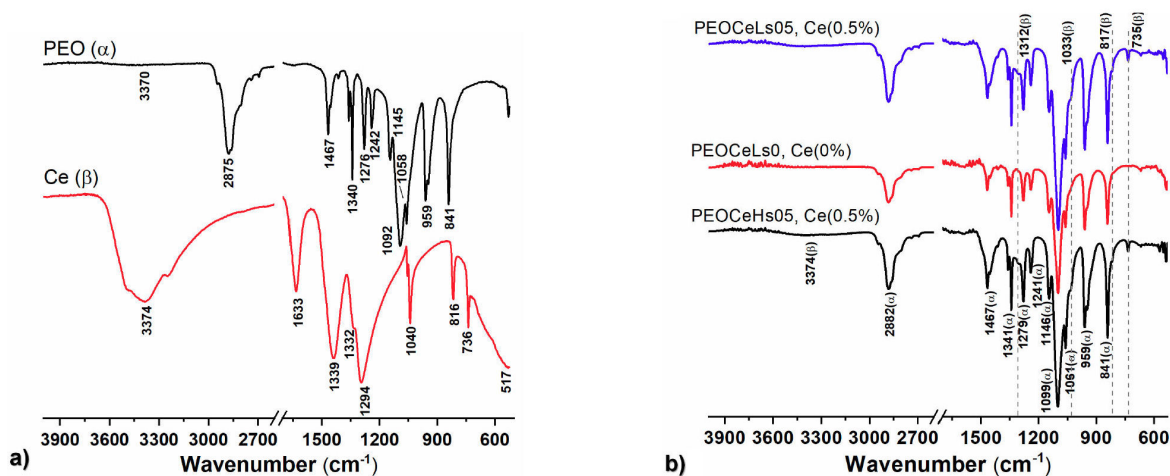

FIGURE 6. FTIR spectroscopy profiles of a) PEO and Ce precursors and b) PEOCeLs0, PEOCeLs05, and PEOCeHs05 electrospun samples.

those corresponding to PEO-Ce single fibers (Fig. 6b)). Two central dominant absorption regions are recognized in all PEO spectra: the first between 3000 and 2700 cm^{-1} and the second from 1500 to 750 cm^{-1} [25].

The width attenuated band centered around 3370 cm^{-1} corresponds to hydroxyl groups (OH-) (Fig. 6b). The band at 2875 cm^{-1} in the precursor suffered a redshift of 4 cm^{-1} assigned to symmetric and asymmetric C-H stretching modes of methyl and methylene groups (-CH$_3$, -CH$_2$-) in all fabricated samples. Two different molecular conformations of PEO, known as helical (H-structure) and transplanar structures (T-structure), have been reported [26–28] in the case of casting PEO films. Adding water to PEO makes complexes with a planar zigzag structure (T) [26]. FTIR result showed, in all cases, a T structure. The bands at 1467, 1340, 1279, and 1242 cm^{-1} were produced due to the wagging and twisting B-vibrations of the -CH$_2$- group, respectively, whereas 959 and 841 cm^{-1} correspond to the -CH$_2$- group under rock-

ing vibration. We used the B-vibration of the -CH$_2$- group at 1467 cm^{-1} as a reference since it has been suggested that neither the intensity nor the position is affected by the conformation and crystallinity of PEO [29, 30]. The vibrational bands at 1340, 1279, 959, and 841 cm^{-1} were characteristic of the H structure, whereas 1340, 1242, and 959 cm^{-1} were characteristic of the T structure [26]. In turn, 1145, 116, and 1062 cm^{-1} bands were associated with C=O asymmetric stretching vibration of secondary and primary alcohols, indicating the crystallinity of PEO. The redshift of about 17 cm^{-1} at 1099 cm^{-1} peak suggests that chain-chain interactions may be due to a restraint stretching vibration of the -C-O-C- group in the main chain [31]. On the other hand, Fig. 6a also shows the cerium (III) nitrate hexahydrate (Ce) precursor FTIR spectra. In particular, the broad OH- band around 3374 cm^{-1} and the NO$_3$-(H$_2$O)$_6$ ions at A (1050-1550 cm^{-1}) and B (1550-1700 cm^{-1}) vibrational bands were observed. Band A at 1340 and 1349 cm^{-1} corresponds to the
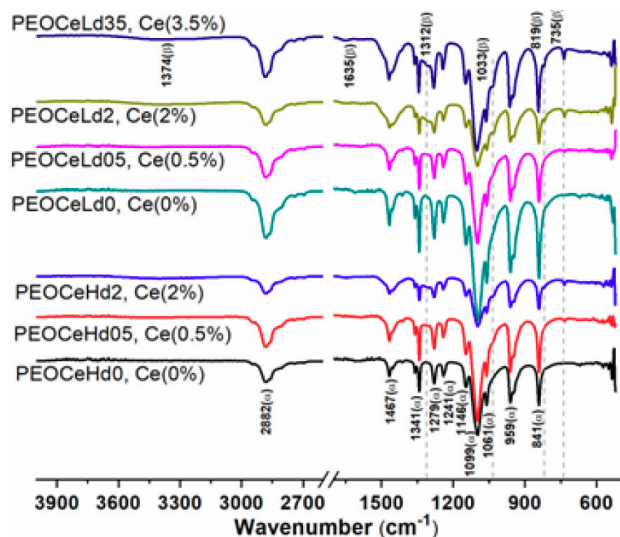
FIGURE 7. FTIR spectra of core-shell electrospun samples at two relative humidities.

NO_3-antisymmetric stretching mode v_3, whereas the water bending mode is observed at 1670 cm^{-1} [32]. As it is suggested by Goebbert *et al.* [32], the splitting of NO_3- antisymmetric stretching mode v_3 is due to the presence of water content at $Ce(NO_3)_3 \cdot 6H_2O$. In contrast, the blueshifts of water modes depend on the reaction with other species, like Ce^{3+} ions. The characteristic bands of the Ce-O and ν(O-CeO) modes were found at 1294, 1040, and 517 cm^{-1}, respectively, whereas 816 and 736 cm^{-1} vibrations are attributed to the envelope phonon band of Ce-O species [33, 34]. After electrospun of single PEO/Ce solutions, the absorbance bands correspond mainly to PEO polymer; due to the low amount of Ce during the preparation of PEOCeHs05 and PEOCeLs05 samples. Small characteristic broadbands of Ce-O modes at 1312, 1033, 817, and 735 cm^{-1} were found.

Core-shell (PEO-PEO/Ce) system. Figure 7 shows the FTIR spectra of the PEO-PEO/Ce electrospun samples at two different relative humidities. As in the case of single fibers, all absorbance bands correspond manly to the PEO polymer. The characteristic broadbands of Ce-O modes at 1312, 1033, 817, and 735 cm^{-1} were found. A higher transmittance is appreciated when the Ce amount increases, particularly at 735 cm^{-1} (Fig. 7).

3.3. Thermal analysis

The determination of future applications of the membranes depends, among others, on their thermal properties. Figure 8 shows the thermal analysis of all electrospun membranes. Differential scanning calorimetry (DSC, Fig. 8a)) was carried out to determine the effect of Ce dopant on the crystallinity of single and core-shell PEO samples. Figure 12 corresponds to the obtained individual endothermal temperature T_m of the precursors, 57.8 and 69.4°C for Ce dopant and PEO, respectively. The crystallinity percentage χ_C of all samples was determined by $\chi_C = (\Delta H_m / \Delta H_m^o) \times 100\%$
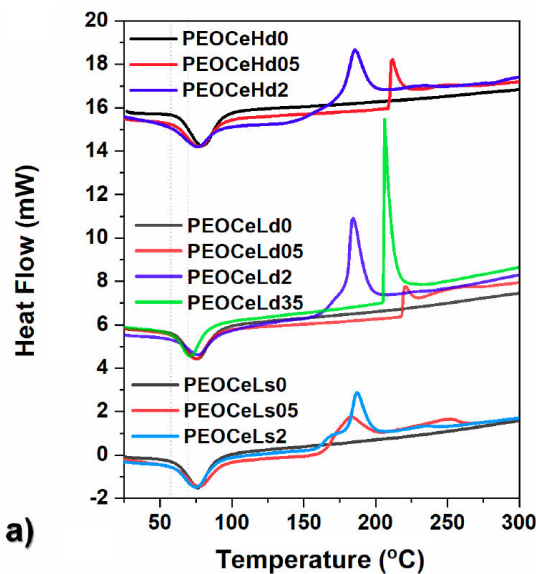
a)
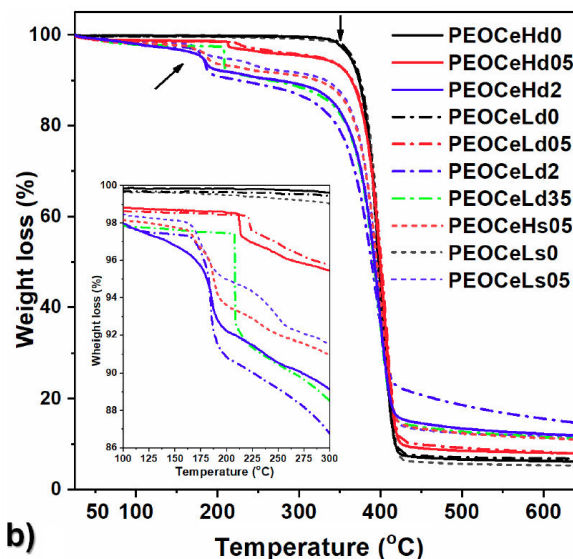
b)

FIGURE 8. Thermal properties of single and core-shell samples. a) DSC and b) TGA spectra.

and $\chi_C = (\Delta H_m / (1 - \alpha) \Delta H_m^o) \times 100\%$, for the undoped and doped fibers, respectively. ΔH_m is the experimental enthalpy of the membranes, $\Delta H_m^o \cdot (196.8$ J/g) the melting enthalpy reference of 100 % crystalline PEO and α the fraction of the Ce dopant [35].

In all fiber samples, an increment of Tm is observed independently of Ce amount. Single fibers (Fig. 8a)) showed a shift of ~ 6°C when they were electrospun, whereas coreshell ones presented increments of ~ 1.9 and ~ 7.7° for the samples with the higher and lower amount of Ce (PEO-CeLd35 and PEOCeHd05), respectively. Single fibers have shown negligible changes between doped and undoped samples or ambient water molecules during the fabrication process (% RH). By its side in core-shell fibers, a relationship of Tm with the concentration of Ce and ambient water molecules (% RH) is observed. Samples fabricated with 27-32 %RH showed an increase in their T_m, under a 3.5 %
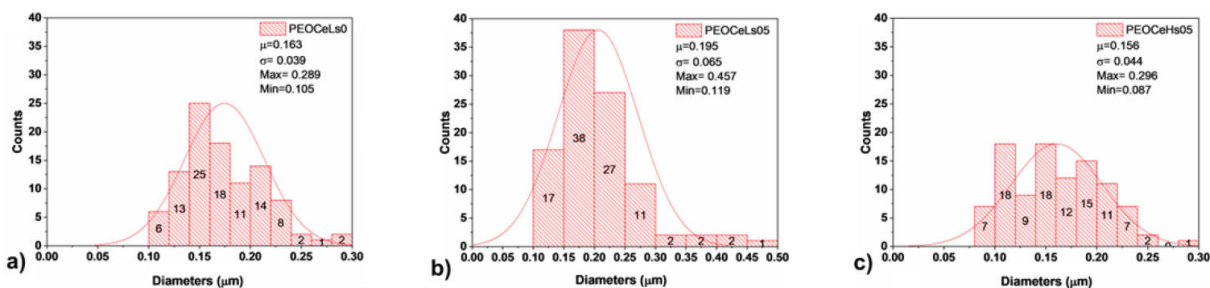
FIGURE 9. Average diameter of single samples. a) PEOCeLs0, b) PEOCeLs05, and c) PEOCeHs05.
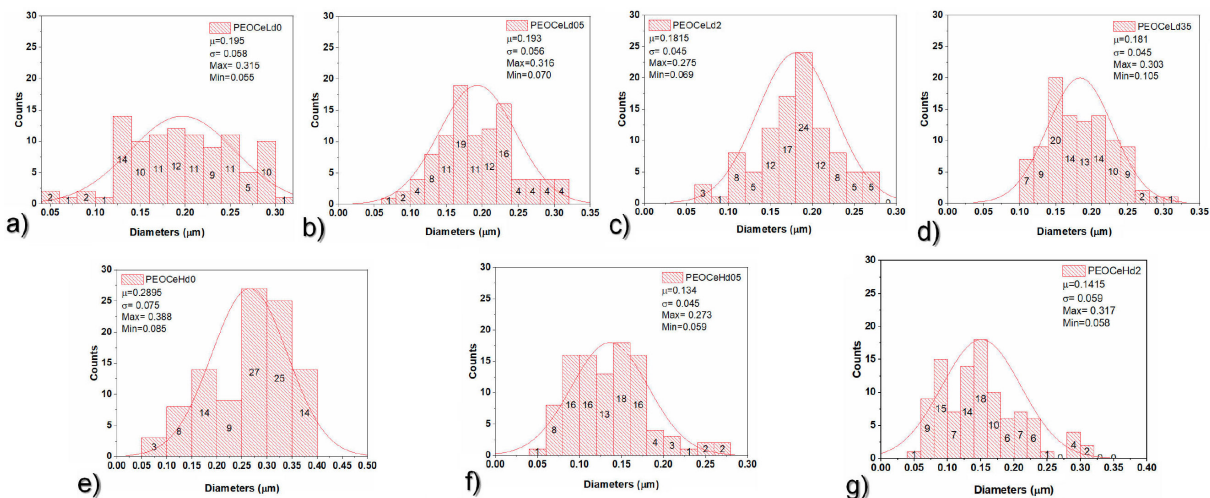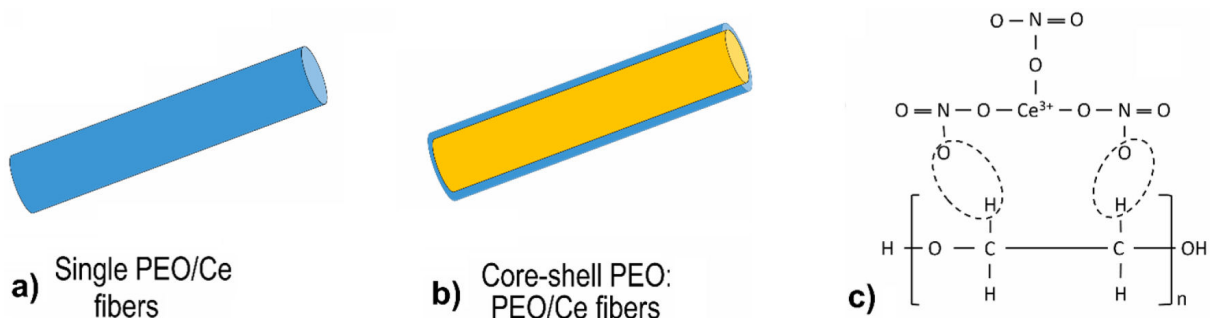

FIGURE 10. Average diameter of core-shell samples. a) PEOCeLd0, b) PEOCeLd05, c) PEOCeLd2, d) PEOCeLd35, e) PEOCeHd0, f) PEOCeHd05, and g) PEOCeHd2.


FIGURE 11. Schematic diagram of a) single PEO/Ce fiber (blue), b) cross-section of core-shell PEO: PEO/Ce fiber. PEO/Ce fiber in blue and PEO fiber in yellow, and c) ionic interaction between (-CH$_2$CH$_2$O-)n chain and Ce(NO$_3$)$_3$ 6H$_2$O.

amount of Ce dopant. The opposite behavior was presented in the fibers fabricated at 47-52 %RH. Table II shows the thermal variables obtained by DSC and TGA of all single and core-shell fabricated samples, including melting T_m, melting enthalpy variation ΔH_m, fractional crystallinity χ_C, the degradation temperatures T_d, and the correspondent weight lost during the degradation process. In concordance with previous reports, the undoped single or core-shell fibers presented a crystallinity ranging from 52.7 to 54.2 % [36]. A slight increment was observed for the PEOCeHd0 core-shell membrane fabricated at 27-32 %RH.

It has been reported that a PEO fiber contains several fibrils of fibrillar crystals and amorphous regions [36, 37]. The addition of Ce(NO$_3$)$_3$·6H$_2$O induces the increment of crystallinity of single and core-shell samples until 2 %, indicating that there is a cut-off dopant concentration above which χ_C decreases (PEOCeLd35 sample). We propose a reaction of one oxygen of NO^{3-} with one hydrogen of -C- chain of PEO throughout hydrogen bridges (Fig. 11c)). The presence of additional moisture during the fabrication process at 47-52 %RH could promote stronger hydrogen bridges during the fabrication process that lead to slight crystallinity increment

TABLE II. Thermal properties of single and core-shell samples, assessed by DSC and TGA.

Sample	T_m (°C)	ΔH_m (J/g)	χ_C (%)	$T_{D \max 1}$ (% lost)	$T_{D \max 2}$ (% lost)	Total % lost
PEOCeLs05	75.4	101.3	54.2	175 (1.71) 182 (1.14) 244 (2.29)	402 (76.6)	81.74
PEOCeLs0	75.3	103.2	52.7	———	403 (93.06)	93.06
PEOCeHs05	74.2	99.8	53.4	166 (0.82) 184 (2.21) 228 (1.26)	402 (76.10)	80.39
PEROCeLd35	71.3	70.3	54.9	174 (1.22) 185(4.48)	398 (63.86)	70.56
PEOCeLd05	75.4	103.1	55.1	222 (0.89)	404 (84.04)	84.93
PEOCeLd0	75.3	105.9	53.8		402 (91.61)	91.61
PEOCeHd2	75.6	91.8	58.3	181 (1.19) 185 (2.09)	398 (71.33)	74.61
PEOCeHd05	77.1	106.2	56.8	211 (1.34)	403 (88.22)	89.56
PEOCeHd0	79.2	106.7	54.2	——-	401 (92.32)	92.32
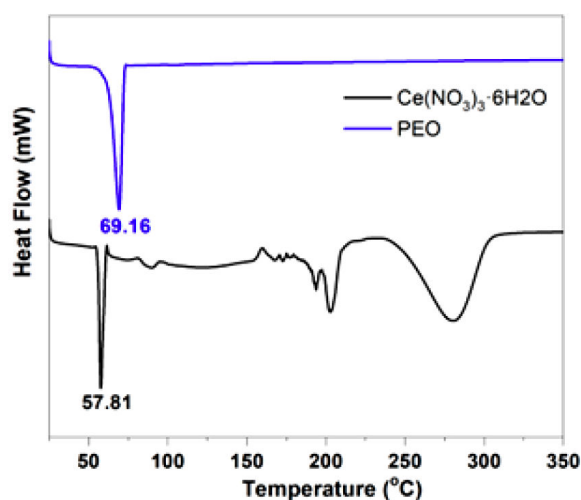
FIGURE 12. Individual endothermal temperature T_m of PEO and Ce(NO$_3$)$_3$6H$_2$O.

in Ce doped core-shell samples vs those fabricated at 27-32 %RH [5].

The thermogravimetric analysis of undoped and doped PEO single and core-shell fibers is presented in Fig. 8b, whereas the first derivative of TGA (DTGA) is supplied as supplementary information (Fig. 13). Doped PEO single fibers DTGA (PEOCeLs05 and PEOCeHs05, Figs. 8b and 12a) revealed three processes of weight loss of $\sim$ 4.3 and $\sim$ 5.1 %, respectively, between 150 and 275°C that could correspond to loss of water, inorganic and organic materials decomposition from PEO and NOx [38–40]. The highest weight loss of doped and undoped samples occurs $\sim$ 400°C, and is related to the PEO [35]. Then, adding Ce dopant enhances the thermal properties of the PEO single fibers and consequently a lower loss of mass, independently of the
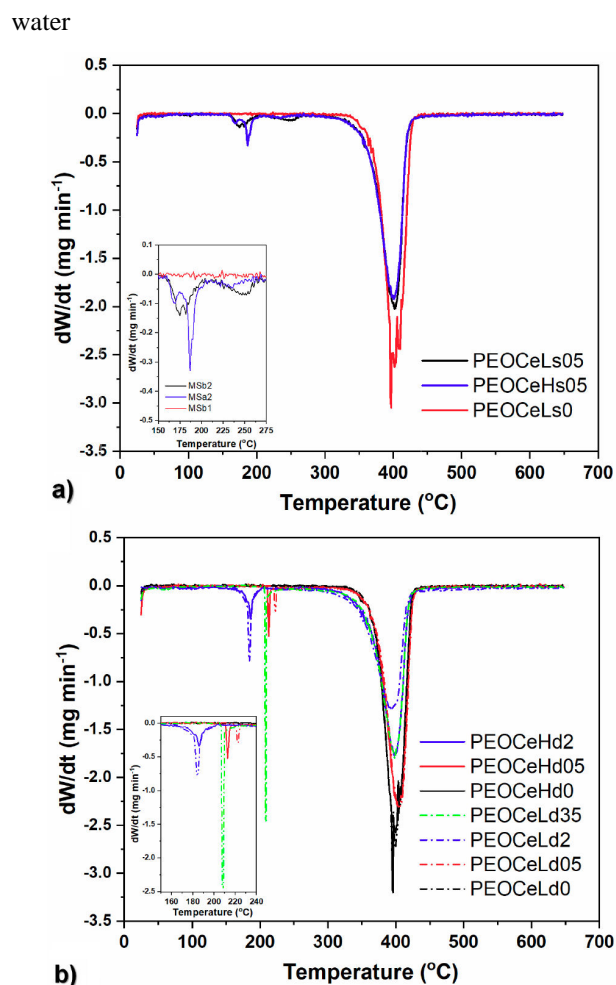

FIGURE 13. The first derivative of TGA of undoped and doped PEO in a) single and b) core-shell fibers.

concentration in the atmosphere during the fabrication. By

its side, core-shell samples PEOCeHd05, PEOCeLd05, and PEOCeLd35 (Figs. 8b) and 12 showed one peak between 200 and 225°C with mass losses close to 1.3, 1.0, and 11.6, respectively. PEOCeHd2 and PEOCeLd2 presented two mass loss steps at 160-205°C of $\sim$ 3.3 and $\sim$ 7 %, respectively. As in the case of single fiber samples, the highest weight loss of doped and undoped samples is related to the PEO [35]. A coating of PEO on Ce-PEO fibers improves their thermal properties until a concentration of 2.0 %(m/v) with a lower loss of mass, independently of the water concentration in the atmosphere during the fabrication. In both cases, single or core-shell Ce doped fibers, beyond 425-430°C a small amount of weight loss could be observed, indicating the remaining transformation of PEO into carbonaceous products as well as leading to the formation of cerium oxide, as was corroborated by FTIR and DSC [38, 39].

4.   Conclusions

This study established the experimental conditions to fabricate cerium doped and undoped PEO single and core-shell fibers. Thinner single fibers were obtained when moisture ambient increases from 27-32 to 47-52 %RH, independent of Ce dopant amount. However, the thinnest average fiber diameter was found at 47-52 %RH, adding 2% of dopant. The use of cladding (shell fiber) allows the increment of cerium in the inner matrix (core-fiber) to produce non-beading continuous fibers with 3.5% of the dopant. In concordance with previous reports, the undoped single or core-shell fibers presented a crystallinity ranging from 52.7 to 54.2%. The use of cerium dopant up to 2% induces an increase in their crystallinity due to the formation of Ce-O species, enhancing their thermal properties, regardless of the moisture during manufacturing.

Acknowledgements

1. Y. Li, X. Y. Yang, Y. Feng, Z. Y. Yuan, and B. L. Su, One-Dimensional Metal Oxide Nanotubes, Nanowires, Nanoribbons, and Nanorods: Synthesis, Characterizations, Properties and Applications, *Crit. Rev. Solid State* **37** (2012) 1, https://doi.org/10.1080/10408436.2011.606512.

2. R. M. Nezarati, M. B. Eifert, and E. Cosgriff-Hernandez, Effects of Humidity and Solution Viscosity on Electrospun Fiber Morphology, *Tissue Eng. Part C-Me* **19** (2013) 810, https://doi.org/10.1089/ten.tec.2012.0671.

3. T. A. Saleha, P. Parthasarathy, and M. Irfan, Advanced functional polymer nanocomposites and their use in water ultra-purification, *Trends Environ. Anal. Chem.* **24** (2019) e00067, https://doi.org/10.1016/j.teac.2019.e00067.

4. S. De Vrieze, T. Van Camp, A. Nelvig, B. Hagstrom, P. Westbroek, and K. De Clerck, The effect of temperature and humidity on electrospinning, *J. Mater. Sci.* **44** (2009) 1357, http://dx.doi.org/10.1007/s10853-008-3010-6.

5. Y. E. Aguirre-Chagala, V. M. Altuzar-Aguilar, J. G. Domínguez-Chávez, E. F. Rubio-Cruz, and C. O. Mendoza-Barrera, Influence of Relative Humidity on The Morphology of Electrospun Polymer Composites, *Der Chem. Sinica* **8** (2017) 83, https://www.imedpub.com/articles/influence-of-relative-humidity-on-the-morphology-of-electrospun-polymercomposites.php?aid=18380.

6. T. A. Saleha, P. Parthasarathy, and M. Irfan, Advanced functional polymer nanocomposites and their use in water ultra-purification, *Trends Environ. Anal.* **24** (2019) e00067, https://doi.org/10.1016/j.teac.2019.e00067.

7. N. Thakur, P. Manna, and J. Das, Synthesis and biomedical applications of nanoceria, a redox active nanoparticle, *J. Nanobiotechnol.* **17** (2019) 84, https://doi.org/10.1186/s12951-019-0516-9.

8. J. Pelipenko, J. Kristl, B. Janković, S. Baumgartner, and P. Kocbek, The impact of relative humidity during electrospinning on the morphology and mechanical properties of nanofibers, *Int. J Pharmaceut.* **456** (2013) 125, https://doi.org/10.1016/j.ijpharm.2013.07.078.

9. C. I. Williams *et al.*, Cerium(III) Nitrate Containing Electrospun Wound Dressing for Mitigating Burn Severity, *Polymers.* **13** (2021) 3174, https://doi.org/10.3390/polym13183174.

10. H. Boudellioua, Y. Hamlaoui, L. Tifouti, and F. Pedraza, Effects of polyethylene glycol (PEG) on the corrosion inhibition of mild steel by cerium nitrate in chloride solution. *Appl. Surf. Sc.* **473** (2019) 449, https://doi.org/10.1016/j.apsusc.2018.12.164.

11. M. Zatoń, J. Rozière, and D. J. Jones, Mitigation of PFSA membrane chemical degradation using composite cerium oxide-PFSA nanofibres, *J. Mater. Chem. A* **5** (2017), 5390, https://doi.org/10.1039/c6ta10977b.

12. M. Richard-Lacroix and C. Pellerin, Raman spectroscopy of individual poly(ethylene oxide) electrospun fibers: Effect of the collector on molecular orientation, *Vib. Spectrosc.* **91** (2017) 92, https://doi.org/10.1016/j.vibspec.2016.09.002.

13. C. Lu *et al.*, Thermal conductivity of electrospinning chain-aligned polyethylene oxide (PEO), *Polymer* **115** (2017) 52, https://doi.org/10.1016/j.polymer.2017.02.024.

14. J. A. Ajao, A. A. Abiona, S. Chigome, A. Y. Fasasi, G. A. Osinkolu, and M. Maaza, Electric-magnetic field-induced aligned electrospun poly (ethylene oxide) (PEO) nanofibers, *J. Mat. Sci.* **45** (2010) 2324, `https://doi.org/10.1007/s10853-009-4196-y`.

15. X. Liu *et al.*, Fabrication and Properties of 5% Ce-Doped BaTiO3 Nanofibers-Based Ceramic, *J. Electron. Mater.* **47** (2018) 1099, `https://doi.org/10.1007/s11664-017-5862-5`.

16. G. Kwak, G. H. Lee, S. H. Shim, and K.B. Yoon, Fabrication of Light-Guiding Core/Sheath Fibers by Coaxial Electrospinning, *Macromol. Rap. Commun.* **29** (2008) 815, `https://doi.org/10.1002/marc.200800065`.

17. M. Richard-Lacroix and C. Pellerin, Raman spectroscopy of individual poly(ethylene oxide) electrospun fibers: Effect of the collector on molecular orientation, *Vib. Spectrosc.* **91** (2017) 92, `https://doi.org/10.1016/j.vibspec.2016.09.002`.

18. J. H. Yu, S. V. Fridrikh, and G. C. Rutledge, Production of Submicrometer Diameter Fibers by Two-Fluid Electrospinning, *Adv. Mater.* **16** (2004) 1562, `https://doi.org/10.1002/adma.200306644`.

19. R. Sharma, N. Singh, S. Tiwari, S. K. Tiwari, and S. R. Dhakate, Cerium functionalized PVA-chitosan composite nanofibers for effective remediation of ultra-low concentrations of Hg(II) in water, *RSC Adv.* **5** (2015) 16622, `https://doi.org/10.1039/c4ra15085f`.

20. R. S. McLean and B. B. Sauer, Tapping-Mode AFM Studies Using Phase Detection for Resolution of Nanophases in Segmented Polyurethanes and Other Block Copolymers, *Macromolecules* **30** (1997) 8314, `https://doi.org/10.1021/ma970350e`.

21. Z. Sun, E. Zussman, A. L. Yarin, J. H. Wendorff, and A. Greiner, Compound core-shell polymer nanofibers by co-electrospinning, *Adv. Mater.* **15** (2003) 1929, `https://doi.org/10.1002/adma.200305136`.

22. T. Kim *et al.*, Highly Reproducible Thermocontrolled Electrospun Fiber Based Organic Photovoltaic Devices, *ACS Appl. Mater. Interfaces* **7** (2015) 4481, `https://doi.org/10.1021/am508250q`.

23. P. Su *et al.*, Electrospinning of chitosan nanofibers: The favorable effect of metal ions, *Carbohydr. Polym.* **84** (2011) 239, `https://doi.org/10.1016/j.carbpol.2010.11.031`.

24. A. Z. Wang, W. Ye, X. Luo, and Z. Wang, Fabrication of Superhydrophobic and Luminescent Rare Earth/Polymer complex *Films, Sci. Rep.* **6** (2016) 24682, `https://doi.org/10.1038/srep24682`.

25. S. Yang, Z. Liu, Y. Liu, and Y. Jiao, Effect of molecular weight on conformational changes of PEO: an infrared spectroscopic analysis, *J. Mater. Sci.* **50** (2015) 1544, `https://doi.org/10.1007/s10853-014-8714-1`.

26. J. I. Marcos, E. Orlandi, and G. Zerbi, Poly(ethylene oxide)-poly(methyl methacrylate) interactions in polymer blends: an infra-red study, *Polymers-Basel* **31** (1990) 1899, `https://doi.org/10.1016/0032-3861(90)90014-P`.

27. F. Gu, H. Bua, and Z. Zhang, A unique morphology of freeze-dried poly(ethylene oxide) and its transformation, *Polymers-Basel* **41** (2000) 7605, `https://doi.org/10.1016/S0032-3861(00)00139-7`.

28. Y. Takahashi, I. Sumita, and H. Tadokoro, Structural studies of polyethers. IX. Planar zigzag modification of poly(ethylene oxide), *J. Polym. Sci. Pol. Phys.* **11** (1973) 2113, `https://doi.org/10.1002/pol.1973.180111103`.

29. J. Xu, Q. Xiong, G. Liang, X. Shen, H Zou, and W. Xu, Ion-Polymer Interactions in $SmCl3(H_2O)^6$ Doped Poly(ethylene oxide) Electrolytes, *J. Macromol. Sci. B* **48** (2009) 856, `https://doi.org/10.1080/00222340902958778`.

30. G. Liang, J. Xu, W. Xu, X. Shen, H. Zhang, and M. Yao, Effect of filler-polymer interactions on the crystalline morphology of PEO-based solid polymer electrolytes by Y^2O^3 nano-fillers, *Polym. Compos.* **32** (2011) 511, `https://doi.org/10.1002/pc.21058`.

31. C. Bergeron, E. Perrier, A. Potier, and G. Delmas, A Study of the Deformation, Network, and Aging of Polyethylene Oxide Films by Infrared Spectroscopy and Calorimetric Measurements, *Int. J. Spectrosc.* **2012** (2012) ID 432046. `https://doi.org/10.1155/2012/432046`.

32. D. J. Goebber *et al.*, Infrared Spectroscopy of the Microhydrated Nitrate Ions $NO^3\text{-}(H^2O)1\text{-}6$, *J. Phys. Chem. A* **113** (2009) 7584, `https://doi.org/10.1021/jp9017103`.

33. L. Marzi *et al.*, Cytotoxicity and Genotoxicity of Ceria Nanoparticles on Different Cell Lines in Vitro, *Int. J. Mol. Sci.* **14** (2013) 3065, `https://doi:10.3390/ijms14023065G`.

34. Jayakumar, A. A. Irudayaraj, and A. D. Raj, Investigation on the synthesis and photocatalytic activity of activated carbon-cerium oxide (AC-CeO^2) nanocomposite, *Appl. Phys. A* **125** (2019) 742, `https://doi.org/10.1007/s00339-019-3044-4`.

35. K. A. Narh, L. Jallo, and K. Y. Rhee, The effect of carbon nanotube agglomeration on the thermal and mechanical properties of polyethylene oxide, *Polymer Composites*, **29** (2008) 809, `https://doi.org/10.1002/pc.20567`.

36. C. Lu *et al.*, Thermal conductivity of electrospinning chain-aligned polyethylene oxide (PEO), *Polymer* **115** (2017) 52, `http://dx.doi.org/10.1016/j.polymer.2017.02.024`.

37. Y. T. Shieh, G. L. Liu, K. C. Hwang, and C. C. Chen, Crystallization, melting and morphology of PEO in PEO/MWNT-g-PMMA blends, *Polymer* **46** (2005) 10945, `https://doi.org/10.1016/j.polymer.2005.09.022`.

38. A. A. Baqer *et al.*, Synthesis and characterization of binary (CuO)0.6(CeO^2)0.4 nanoparticles via a simple heat treatment method, *Results in Physics* **9** (2018) 471, `https://doi.org/10.1016/j.rinp.2018.02.079`.

39. S. Phoka, P. Laokul, E. Swatsitang, V. Promarak, S. Seraphin, and S. Maensiri, Synthesis, structural and optical properties of CeO^2 nanoparticles synthesized by a simple polyvinyl pyrrolidone (PVP) solution route, *Materials Chemistry and Physics* **115** (2009) 423, `https://doi.org/10.1016/j.matchemphys.2008.12.031`.

40. C. Hernandez *et al.*, Performance evaluation of Ce3+ doped flexible PVDF fibers for efficient optical pressure sensors, *Sensors and Actuators A: Physical* **298** (2019) 111595, `https://doi.org/10.1016/j.sna.2019.111595`.